RESEARCH ON THERMAL ENVIRONMENT ANALYSIS OF PHOTOVOLTAIC POWER PLANTS BASED ON REMOTE SENSING IMAGES

HongLiang Cheng [1], He Huang[1], Junxing Yang [1] *, Ran Pang [2] , JunYang Bian[1]

[1] School of Geomatics and Urban Spatial Informatics, Beijing University of Civil Engineering and Architecture, Beijing, China-2108570021062@bucea.edu.cn,huanghe@bucea.edu.cn,yangjunxing@bucea.edu.cn, bjy1066702005@163.com
[2] Beijing Institute of Surveying and Mapping, Beijing,China-510723874@qq.com

KEY WORDS: Remote sensing image, Photovoltaic power station, Land cover, LST, Spatial analysis.

ABSTRACT:

As a representative of new energy, photovoltaic power stations have developed rapidly in China, with annual installed capacity increasing. At present, research on photovoltaic power plants mainly concentrates on carbon neutrality based on the whole life cycle, and there are few studies on the thermal environment problems that may be caused by photovoltaic power plants. This paper takes the area where the photovoltaic power station is located in Quyang County, Baoding City, Hebei Province, and the surrounding mountains as the research area. It uses Gaofen-1 and Landsat 8 remote sensing images to study the changes in land cover and surface temperature before and after the construction of mountain photovoltaic power stations over a period of 8 years from 2013 to 2020.
Given the lack of quantitative research on the impact of mountain photovoltaic power stations on the surrounding environment using remote sensing technology, this paper focuses on the influence of the distribution and proportion of mountain photovoltaic power stations on the spatial pattern of the thermal environment in the region. Through experimental verification and result analysis, it can be seen that under the geographical location and time conditions of the study area, the proportion of photovoltaic power stations shows a strong correlation with the average surface temperature, which is one of the main factors causing the temperature rise in mountainous areas. It is a land cover type with heat island effects in the traditional sense.

1. INTRODUCTION

With climate change and the depletion of major energy resources, China's focus on energy development and utilization is gradually shifting from fossil fuels to renewable energy. As a representative of renewable energy, solar photovoltaic (PV) power stations have been rapidly developing in China, with the cumulative installed capacity reaching 306.56 GW by 2021. PV power stations in China are mainly concentrated in the northwest, central, and eastern regions. The northwest provinces have abundant solar resources and large areas of desert and semi-desert land, which are suitable for the construction of PV power stations. The central and eastern regions of China are economically developed with high electricity demand, and their PV installation capacity also ranks among the top in the country (Zhang et al., 2018). However, unlike the vast desert areas in the northwest, the central and eastern regions of China do not have large areas of desert land that can be transformed into industrial land suitable for PV power station construction. Instead, PV power stations in these regions are built according to their characteristics. The large-scale construction of PV power stations is bound to have certain impacts on the ecological environment of these regions.

Currently, research on the ecological environmental impacts of solar power station construction mainly focuses on aspects such as energy balance and radiation, carbon emissions, and land use. However, there is relatively less research on the impact of solar power station construction on the thermal environment. Genchi Y et al. developed a thermal balance model for photovoltaic panels based on temperature data obtained from field measurements. The model was used to assess the thermal effects of large-scale rooftop solar panels in the Tokyo area. The results indicated that the construction of rooftop solar panels did not have a significant impact on the urban heat island effect （Genchi et al.,2003） . Nemet G.F. et al. analyzed the extent to which dark-colored photovoltaic panels reduce surface albedo by a series of equations and calculated the radiative forcing generated by solar photovoltaic plants replacing traditional fossil fuels in terms of capacity. This study confirmed that the construction of photovoltaic power plants does alter surface albedo(Nemet et al.,2009). Zhai H. et al. simulated the impact of desert photovoltaic power plants on local wind field intensity and direction at the site, and the results indicated that the construction of photovoltaic power plants reduces wind speed in the downwind direction(Zhai et al.,2012). Yang L.W. conducted field observations in 2015 to investigate the influence of the construction and operation phases of Golmud photovoltaic power plants on meteorological elements. The results demonstrated that the photovoltaic power plants reduced surface temperature at the site. Furthermore, through simulation experiments, it was proven that the photovoltaic power plants also moderately decrease air temperature within a 2m range(Yang,2015). Li S. et al. selected three different photovoltaic power plants in three cities worldwide as study subjects and evaluated the impact of large-scale photovoltaic power plant construction on local climate using quantitative remote sensing methods. The results indicated that appropriate construction and deployment of large-scale photovoltaic power plants in semi-arid and arid regions with low annual precipitation can reduce adverse effects and have a positive impact on the local climate environment(Li et al.,2017). Yin D.Y. et al. conducted field observations on the Gonghe photovoltaic power plant in Qinghai Province and compared the

* Corresponding author

observation data from an automatic weather station with the basic meteorological elements at the control group photovoltaic power plant. The results showed that the construction and installation of photovoltaic power plants reduced soil temperature and increased humidity in desert areas, while also leading to a more uniform wind direction within the site and reducing the probability of high wind speeds(Yin et al.,2017). Broadbent A.M. et al. conducted on-site observations at the RedRock photovoltaic power plant in the United States, and the study indicated that the construction of photovoltaic power plants increased daytime temperatures within a 1.5m range by 1.38 ℃ , with no significant difference in nighttime temperatures(Broadbent et al.,2019).

Surface temperature is the result of the interaction between the Earth's surface and the atmosphere, specifically the exchange of energy between them. Surface temperature is involved in many biophysical processes such as photosynthesis and evapotranspiration and is an important indicator of surface conditions. Different land cover types have different abilities to absorb and reflect solar radiation, so changes in land cover often lead to changes in surface temperature. For example, in the process of urbanization, natural land cover dominated by vegetation is replaced by impervious surfaces such as artificial structures, altering the thermodynamic properties of the underlying surface. Therefore, combining land cover changes with changes in surface temperature and constructing a linear relationship model between them is beneficial for in-depth research on regional ecological and environmental changes. Currently, there is limited research on the thermal environment around photovoltaic power plants. Therefore, this study will conduct a linear regression analysis and spatial analysis of land cover changes and changes in surface temperature before and after the construction of photovoltaic power plants, aiming to explore the impact of photovoltaic power plant construction on the thermal environment in the study area. This research will provide a reference for future photovoltaic project site selection, construction, and addressing thermal environmental issues related to photovoltaic power plants.

2. MATERIALS

2.1 Study Area

The study area is located in Quyang County, southwest of Baoding City, Hebei Province, at the eastern foot of the Taihang Mountains. It has geographical coordinates ranging from 38°26′48″ to 38°57′18″ north latitude and 114°24′30″ to 114°53′54″ east longitude, as shown in Figure 1. Quyang County is characterized as a hilly region, with the overall terrain being higher in the northwest and lower in the southeast. The landforms transition from mountains to hills and then to plains in a northwest-to-southeast direction. Quyang County experiences a semi-humid and semi-arid continental monsoon climate. It has distinct seasons with simultaneous rainfall and heat. The frost-free period lasts for about 190 days. The average annual temperature ranges from 11 to 12.7°C, and the average annual precipitation is around 550mm. The average annual wind speed is 2.3m/s, with a predominance of north winds. Quyang County enjoys abundant sunshine, with an annual average solar radiation exceeding 5040MJ/m2. The average annual sunshine duration exceeds 2600 hours, resulting in a sunshine ratio of 59%(National Bureau of Statistics of China,2021). The vegetation in Quyang County belongs to temperate vegetation, which is relatively simple and mainly consists of mountain shrubs, grasses, and meadows.

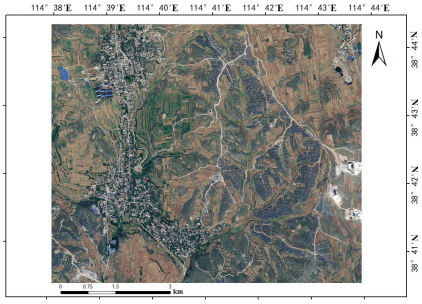

Fig 1. The geographical location of the study area

The photovoltaic power station project under study commenced at the end of 2013. It is divided into five phases to construct a 200,000 kW photovoltaic power station, utilizing nearly 8 km2 of barren hills and slopes. At that time, it was the largest mountainous centralized photovoltaic power station in China(Feng,2015). The central geographical coordinates of the project site are 38°42′43″ north latitude and 114°41′8″ east longitude. The land type in the area where the photovoltaic panels are installed mainly consists of shrubs and grassland.

2.2 Data Source and Preprocessing

The study utilized imagery from two remarkable satellites, namely Landsat 8 and Gaofen-1, as the primary data sources. Launched in February 2013, Landsat 8 carried the sophisticated Operational Land Imager (OLI) and Thermal Infrared Sensor (TIRS) onboard. In this study, the OLI and TIRS sensors were utilized to derive temperature inversion results for the photovoltaic power plants and their surrounding areas. Gaofen-1 satellite, launched in April 2013, carried a remarkable panchromatic and multispectral camera, capable of capturing remote sensing images with a spatial resolution of 2m and an impressive imaging swath of 60km. Leveraging the imagery from this satellite, the study aimed to extract valuable insights into land cover changes within the research area. Through meticulous data processing and analysis, these satellite images were transformed into valuable information, enabling the exploration of temperature patterns and land cover dynamics in and around the photovoltaic power plants.

Located in the northern region of China, Quyang County experiences abundant rainfall during the summer season. However, in the early 2010s, the region suffered from severe air pollution, particularly during the winter and spring seasons, leading to frequent haze and smog episodes. Therefore, this study opted for the autumn season, known for its favorable weather conditions, as the time frame for image acquisition, specifically focusing on late October and early November. The choice of 2013, 2015, and 2020 as the three stages for this study was based on the construction timeline of the photovoltaic power plants in Quyang County. Construction of the power plants began at the end of 2013, with the completion of the first three phases in 2015 and the fourth and fifth phases in 2018. Therefore, the selected image acquisition years correspond to the stages of pre-construction, ongoing construction, and near completion of the photovoltaic power plants. This selection enables a better representation of the land surface and land cover types, facilitating the observation of the impact of the photovoltaic power plants on the surrounding thermal environment as a variable. The imaging times of the two remote sensing images are detailed in Table 1.

Parameters	Data Source

	Landsat 8	Gaofen-1
Imaging time	2013/10/26	2013/11/7
	2015/11/2	2015/11/2
	2020/10/23	2020/11/11

Table 1. Remote sensing image acquisition time

To facilitate visual interpretation, selection of areas of interest, extraction of vegetation index and building index, as well as surface temperature inversion, data preprocessing of remote sensing images is required in this study. Gaofen-1 belongs to the L1 level product and can be orthorectified without control points using the built-in RPC file (rational function model). The elevation data used is the DEM data with a spatial resolution of 900m provided by ENVI 5.3. Atmospheric radiometric calibration was performed on Landsat 8 and Gaofen-1 images using ENVI 5.3 to obtain reflectance data for each band and rescale it to the range of 0-10000. To obtain high-resolution multispectral images, the Gram-Schmidt method was used to perform spectral sharpening fusion processing on the Gaofen-1 image, resulting in a fusion image with a spatial resolution of 2m.

3. RESEARCH CONTENT

3.1 Land Cover Classification and Accuracy Evaluation

To better reflect the characteristics of land use in the study area, this article divides the study area into six land types based on the visual interpretation of high-definition maps. These include vegetation, plowland, bareland, water, photovoltaic power stations, and other structures (excluding photovoltaic power stations, mainly buildings, and roads). In this study, three high-resolution remote sensing images captured by the Gaofen-1 satellite were used as the main data source. The land cover in the study area was classified using the maximum likelihood method in ENVI 5.3, and the results of the land cover classification for three periods are shown in Figure 2. In addition, the area of each land use was calculated using ArcGIS 10.1, as shown in Figure 3.

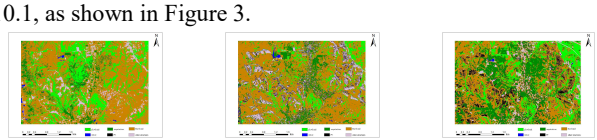

(a) 2013 (b) 2015 (c) 2020

Fig 2. The land cover classification results

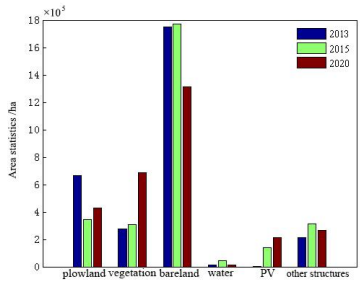

Fig 3 Land cover classification results area statistics

The accuracy evaluation of the classification results is the premise to judge the reliability of the classification results. The most commonly used accuracy evaluation method is the confusion matrix method. In this article, several random points are set on the classified images, and high-definition images that match the date of remote sensing image acquisition in Google Earth Pro are used as references to judge the consistency between the classification results and the high-definition map, and calculate the confusion matrix. The Kappa coefficient is then calculated using this matrix. It is found that the Kappa coefficients of the land cover classification results in three periods are 0.893, 0.882, and 0.923, respectively. The classification errors mainly occur in the confusion between photovoltaic power plants and other structures, the confusion between mountain shadows and water bodies, and the confusion between plowland and bareland. Overall, the land cover classification results are relatively accurate and can be used for further research and analysis.

3.2 Analysis of Spatial Pattern Changes in The Study Area

To analyze the spatial pattern changes in the research area before and after the construction of photovoltaic power plants, this article used ArcGIS 10.1 to calculate the land cover classification results for three phases and the changes in land cover types, as shown in Figure 4.

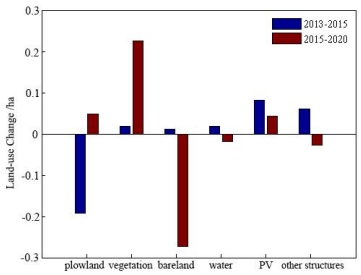

Fig 4. Land cover classification results -land type changes

Land-use transfer matrix can not only reflect the area data of different land classes in fixed regions and fixed periods but also reflect the more abundant area transfer out of each land class in the initial stage and the transfer into the area of each land class in the final stage. Therefore, this study also calculated the land use transfer matrix for the years 2013 and 2020. The calculated land use transfer matrix is shown in Table 2.

Through the analysis of land cover change information and calculation of the land use transfer matrix, it can be observed that there have been significant changes in land cover within the study area from 2013 to 2020. The main changes include: with the development of photovoltaic power station projects, the area of photovoltaic land has greatly increased, mainly occupying the regions that were previously bareland and plowland. The proportion of other structures remains relatively stable, while the average proportion of water bodies in the three-phase land cover results is only 2.48%, and its impact on the thermal environment is minimal, so it will not be discussed further.

2013 / 2020	plowland	vegetation	bareland	water	PV	other structures	total
plowland	920.61	304.34	2225.36	33.21	141.41	356.96	3981.89
vegetation	98.41	367.26	1052.26	22.49	33.50	55.03	1628.95
bareland	889.56	1025.79	6805.42	145.27	480.01	1208.64	10554.69
water	4.53	5.00	37.91	14.89	4.59	2.89	69.81
PV	0.37	2.53	3.34	0.29	0.87	1.03	8.43
other structures	145.08	119.77	560.70	26.26	129.62	295.65	1277.08
total	2058.56	1824.69	10685.13	242.40	789.99	1920.21	17521.00

Table 2. Land-use transfer matrix

3.3 Surface Temperature Retrieval

3.3.1 Surface Temperature Inversion and Accuracy Assessment

Based on the atmospheric correction method, we conducted land surface temperature inversion on Landsat 8 remote sensing images of the study area in 2013, 2015, and 2020, and obtained land surface temperature data for the three periods within the study area. The temperature inversion results are shown in Figure 5.

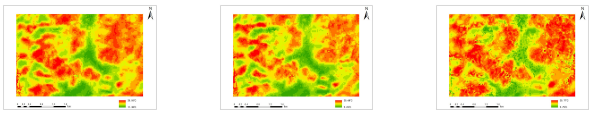

(a) 2013 (b) 2015 (c) 2020

Fig 5. The results of surface temperature retrieval

The minimum temperature, maximum temperature, average temperature, and standard deviation of the third-phase images can be found in Table 3. Combined with the surface temperature inversion results, it can be seen that the red high-temperature areas in the study area are concentrated on the east and west sides. The high-temperature area in the eastern part is compact and close to the north, while the high-temperature area in the western part is scattered and covers a wide range almost from north to south. The surface temperature of the third-phase images in the high-temperature area is concentrated between 23.63℃ and 25.77℃. The surface temperature in the middle belt and southern region of the study area is lower and appears green in the image, with a temperature range mainly between 9.22℃ and 16.79℃. The surface temperature in the yellow medium-temperature area, which is between the high and low temperatures, ranges from 15.73℃ to 22.53℃. Overall, the surface temperature in the study area during this season and period mainly ranges from 9.22℃ to 27.77℃. In the time series, the surface temperature in the study area shows a gradual upward trend over time.

Time	Max /℃	Min /℃	Mean /℃	Standard deviation/℃
2013/10/26	25.55	11.38	18.47	3.17
2015/11/02	25.68	9.22	17.78	3.46
2020/10/23	26.77	16.79	21.78	3.98

Table 3. Surface temperature values of three-phase images

We found from the historical weather website that the highest and lowest temperatures observed at the meteorological station in Baoding on October 26, 2013, November 2, 2015, and October 23, 2020, were 8℃ and 24℃, 8℃ and 25℃, 15℃ and 29℃ respectively. The temperature reported in the weather forecast is the atmospheric temperature near the ground surface, and the heat mainly comes from surface radiation (the heat that warms the atmosphere after the surface absorbs solar radiation and reflects it into the atmosphere). The Landsat 8 remote sensing images used in this section were all taken in mid-October to early November, during the autumn season in North China, where the temperature difference between day and night is large. In addition, the imaging time of the three periods of images is 3:00 UTM (11:00 Beijing time), when the solar radiation is weaker. According to the principle of thermal radiation, the heating and cooling of the surface have a process, so the surface temperature rises slowly at this time and has not reached the maximum value of the day. Furthermore, the surface temperature changes significantly throughout the day, with the morning and evening temperatures being closer to the air temperature. The highest value is reached from noon to afternoon, and the surface temperature in clear summer can reach over 60℃, which is about twice as high as the actual air temperature. Therefore, the surface temperature is usually higher than the local air temperature. From this perspective, the accuracy of our surface temperature inversion is still reliable.

By comparing our experimental results with other remote sensing temperature data and by querying historical weather data, it can be concluded that the surface temperature inversion results in this article are relatively close to the current temperature, which can be used for further research.

3.3.2 Surface Temperature Index Analysis

To further analyze the spatial differences in surface temperature caused by artificial features represented by photovoltaic power stations in the study area and the reasons for their impact, we calculated the Normalized Difference Built-up Index (NDBI) and Normalized Difference Vegetation Index (NDVI) based on Landsat 8 OLI data. Due to the large period of the three-phase images and the fact that theoretically, the image with the highest proportion of photovoltaic power stations should be selected to

better present larger spatial differences, this section focuses on the analysis and study of the most recent image in 2020. By constructing models of the relationship between each index and the change in surface temperature, the influencing factors of surface temperature distribution are quantitatively studied.

Normalized Difference Built-up Index (NDBI) can accurately reflect the information on built-up land, and the values of this index range from -1 to 1. A higher value of NDBI indicates a higher proportion of built-up land and a higher building density in the region. Since it is not possible to distinguish between solar power plants and other structures cover types using Landsat 8 image bands, this study considers them as buildings collectively and conducts a generalized analysis using NDBI. The calculated NDBI results for the study area are shown in Figure 6.

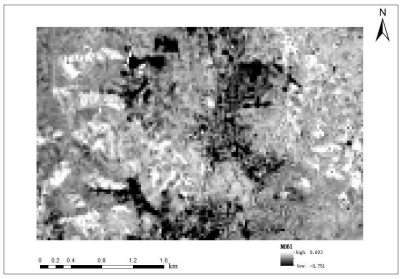

Fig 6. The result of NDBI in the study area

As shown in Figure 6, the high values of NDBI correspond to the first phase site of the photovoltaic power station project, Xiaomu Township County Town in Quyang County, and the site of the third and fourth phases of the photovoltaic power station. These three areas all have concentrated construction and high density. The central and northern regions and the central and southern regions of the study area are mainly vegetation, and the NDBI values corresponding to these areas are relatively low. Overall, the extraction results are consistent with the actual situation, and the spatial distribution characteristics of NDBI are consistent with the results of land surface temperature inversion.

To analyze the relationship between surface temperature and NDBI quantitatively, we generated 2000 random points in the study area, extracted the NDBI values and temperature values at each random point, and then constructed a linear regression equation:

$$LST = 21.66 \times NDBI + 23.64 \quad (1)$$

where LST= land surface temperature
$NDBI$= normalized difference building index

The coefficient of determination R^2 of the regression equation can evaluate the degree of linear correlation between a variable and other variables. The closer its value is to 1, the better the fitting effect of the regression line. Whether the correlation between two variables reaches a significant level needs to be judged by the significance index. If the significance index Sig is less than 0.05, it indicates that the correlation between variables has reached a significant level. In this regression, R^2=0.64 and Sig=0.000, indicating that the surface temperature and NDBI are significantly correlated at the 1% level. As shown in Figure 7, the surface temperature and NDBI are positively correlated, and the surface temperature increases with the increase of NDBI value.

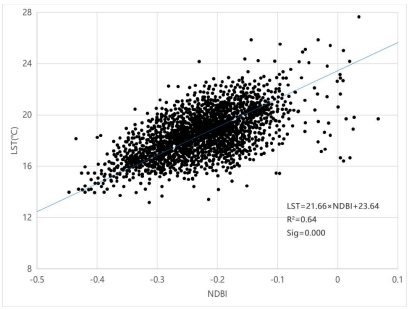

Fig 7. Map of the linear relationship between land surface temperature and NDBI

Normalized Difference Vegetation Index (NDVI) can indicate the growth status and vegetation distribution density of plants. The calculation results of NDVI in the study area are shown in Figure 8.

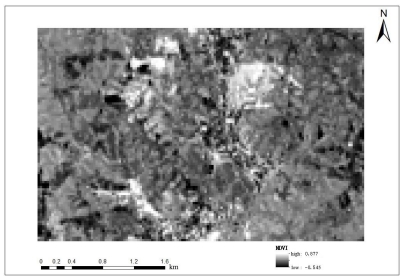

Fig 8. The result of NDVI in the study area

From Figure 8, it can be seen that the lowest values of NDVI appear in the northwest, southwest, and southeast of the study area. These areas are few water bodies in the study area, and the vegetation index of water bodies is relatively low. The distribution of the second lowest values of NDVI is extensive, corresponding to sporadic vegetation interspersed in built-up areas. The highest values of NDVI appear in the central area of the study area, where the land surface is mainly composed of cultivated land, vegetation, and bare land. Comparing the NDVI data with the inversion results of land surface temperature, it can be seen that except for water bodies, the areas with high NDVI values correspond to low-temperature areas, while the areas with low NDVI values correspond to medium and high-temperature areas.

We also generated 2000 random points within the study area, extracted the corresponding NDVI values and land surface temperature results of these random points, and then constructed a linear regression equation:

$$LST = -22.80 \times NDVI + 19.32 \quad (2)$$

where LST= land surface temperature
$NDVI$= normalized difference vegetation index

The calculated R^2 for regression equation (2) is 0.54, Sig=0.000, indicating a significant correlation between land surface temperature and NDVI at the 1% level. From Figure 9, it can be observed that there is a negative correlation between land surface temperature and NDVI, with higher vegetation cover corresponding to lower land surface temperature. Additionally, by comparing the coefficients of linear regression in Figure 7 and Figure 9, it can be inferred that buildings have a greater impact on land surface temperature.

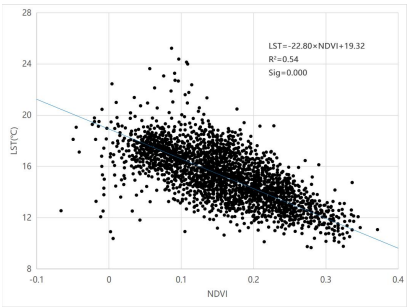

Fig 9. Map of the linear relationship between land surface temperature and NDVI

3.4 Analysis of Hot Environment Space

3.4.1 Spatial Analysis of Thermal Environment in The Study Area

The results analyzed by the normalized difference vegetation index (NDVI) and the normalized difference built-up index (NDBI) indicate that the surface temperature is mainly influenced by the underlying surface properties. This article conducts a visual comparison analysis between the temperature inversion results in 2020 and the land cover classification results in 2020. From Figure 10, it can be seen that except for the southwest corner and northeast corner of the study area, the areas above 22°C in the study area coincide with the distribution of photovoltaic power stations, and the temperature results obtained from the inversion of such land cover types are significantly higher than those of vegetation, bareland, and other areas. The land cover types in the mid-temperature zone are mainly composed of other structures, while the land cover types in the low-temperature zone are mainly vegetation, cultivated land, and a small number of water bodies. The distribution of the low-temperature zone is relatively scattered. Among them, the surface temperature values decrease as they move outward from the center of the photovoltaic power station.

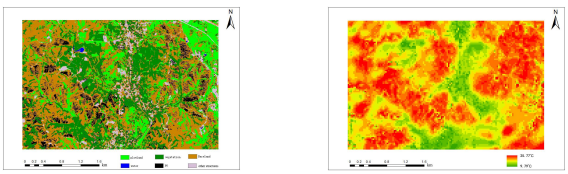

(a) Land cover (b) Temperature inversion

Fig 10. Comparison of land cover and land surface temperature inversion

After statistical calculations, it can be known that the average surface temperature of artificial land area is 20.06℃, among which the average surface temperature of photovoltaic power station area is 24.16℃, the average surface temperature of cultivated land area is 22.63℃, and the average surface temperature of residential area is 19.38℃. Due to the presence of a large amount of vegetation between buildings in the town, the low resolution of the thermal infrared band, and the small size of the buildings, the surface temperature of the buildings in the town is lower than expected. The average surface temperature of the natural land area is 16.61℃, which is 3.45℃ lower than the average surface temperature of the artificial land area, indicating the existence of thermal environmental changes in the study area.

This article classifies the inversion results of surface temperature in 2020 using the standard deviation grading method. The specific grading method is shown in Table 4.

Level	Grading Method
Low-temperature zone	$T < T_{mean} - T_{std}$
Lower temperature zone	$T_{mean} - T_{std} < T < T_{mean} - 0.5T_{std}$
Mid-temperature zone	$T_{mean} - 0.5T_{std} < T < T_{mean}$
Higher temperature region	$T_{mean} < T < T_{mean} + 0.5T_{std}$
High-temperature zone	$T_{mean} + 0.5T_{std} < T < T_{mean} + T_{std}$
Ultra-high temperature zone	$T > T_{mean} + T_{std}$

Table 4. Classification of land surface temperature retrieval results

where T= the surface temperature retrieved from inversion
T_{mean}= The average value of standardized temperature
T_{std}= Standard deviation of standardized temperature

Further, combine the results of land surface temperature classification with land cover classification results. Use zoning statistics and overlay analysis spatial statistical methods to calculate the average land surface temperature of each land cover class in the 2020 image. Also, calculate the proportion of different temperature zones within each land cover class, as shown in Table 5.

Temperature	vegetation	plowland	bareland	water	PV	other structures
Low temperature	24.76	10.45	2.08	81.03	1.23	4.79
Lower temperature	39.79	14.15	21.46	14.30	5.17	10.61
Mid-temperature	24.79	19.27	42.60	3.50	10.52	24.29
Higher temperature	8.31	23.81	21.42	0.90	20.99	25.35
High temperature	1.82	17.92	7.62	0.16	36.26	16.10
Ultra-high temperature	0.52	15.20	4.83	0.11	25.83	18.87

Table 5. The proportion of the area of different temperature levels in different regions in 2020

According to Table 5, the results of sorting various land categories in the study area in 2020 in terms of surface temperature from high to low are as follows: PV, plowland, other structures, bareland, vegetation, and water. The above analysis shows that in the spatial analysis of the thermal environment in the study area, the conclusions of visual comparison, statistical average temperature, and calculation of the area occupied by each land class in temperature zones are consistent with each other.

3.4.2 Analysis of Thermal Environment Space in Photovoltaic Power Plants

To further analyze the impact of the distribution and proportion of photovoltaic power plants on surface temperature changes, this paper first divides the study area into several grids using the fishnet function of ArcGIS software. Then, spatial analysis methods are used to calculate the proportion of each land cover type in each grid in 2020 and calculate the corresponding average temperature data for each grid in 2020. Finally, the correlation between the proportion of photovoltaic power plant land cover and the average surface temperature of the corresponding grid is analyzed using mathematical statistics. Given the small size of the study area and the small number of pixels occupied by photovoltaic power plant land cover, this paper uses a grid size of 210m×210m for research, aiming to explore the relationship between the distribution of photovoltaic power plants and surface temperature changes at a finer spatial scale. We constructed a linear regression equation using the proportion of photovoltaic power stations in each grid and the average surface temperature.

$$mean\ LST = 0.073 * PV + 18.21 \quad (3)$$

where $mean\ LST$=Average surface temperature
PV=Proportion of photovoltaic power plants per grid

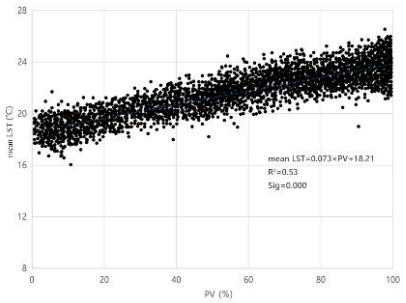

Fig 11. Fitting results of PV power station proportion and mean surface temperature

According to regression equation (3) and Figure 11, it can be seen that there is a strong correlation between the proportion of photovoltaic power plants and the average land surface temperature in the 210m grid. The multiple coefficient of determination R^2 of the regression equation is 0.53, Sig = 0.000, indicating a significant correlation between the two at the 1% level. The linear coefficient is 18.21, indicating a positive correlation between the proportion of photovoltaic power plants and the average land surface temperature. The average land surface temperature increases with the increase in the proportion of photovoltaic power plants. Therefore, the distribution of photovoltaic power plants can reasonably explain the phenomenon of temperature rise on the land surface. In the geographical location and time range corresponding to the remote sensing image (autumn daytime in mid-latitude areas), photovoltaic power plants are one of the main factors causing temperature rise in mountainous areas and are a type of land cover that traditionally has a heat island effect.

We believed that this can be explained from the perspective of the operating characteristics of the photovoltaic power station itself and the large-scale construction of the photovoltaic power station. First, when the photovoltaic power station is operating, it directly converts solar radiation and scattered radiation into electrical energy. There will inevitably be a large amount of heat radiation around the power station, and the individual photovoltaic panels have small areas and small heat capacities. Therefore, the photovoltaic components need to release heat radiation from both the top and bottom, causing a local temperature increase. Second, the large-scale construction of photovoltaic power stations will block the original land surface, forming dark areas on the land surface, and reducing the absorption of heat by the surface soil. The photovoltaic components themselves also absorb light, further reducing the heat absorbed by the land surface, to a certain extent, changing the original surface albedo of the surrounding area. In addition, the construction of photovoltaic power stations will change the original surface roughness, affecting the long-wave radiation received and reflected by the ground, thereby changing the ventilation and heat dissipation conditions around the power station and causing a temperature rise in the surrounding area.

In response to the phenomenon of increased surface temperature in mountainous areas caused by photovoltaic power stations, this paper believes that when planning the layout of photovoltaic power stations, the distance between photovoltaic components can be increased. In this way, after the photovoltaic components are installed, the bare ground under the components can be exposed, thereby playing a relatively cooling effect on mountainous areas. According to the land cover situation in the study area, it can be seen that the land features distributed from inside to outside and from near to far around the photovoltaic power station are other structures, bareland, and vegetation/plowland. Therefore, it can be considered to minimize the distance between the photovoltaic power station and the vegetation while not affecting the normal operation of the power station, to offset the warming effect of the power station with the cooling effect of vegetation. According to the land cover results map for 2020, there is still a considerable amount of bare land in the study area, which corresponds to actual barren mountains and hills resources. Considering the serious hydraulic erosion in the study area, it is possible to guide the development of mountainous fruit and forestry industries, increase the proportion of vegetation coverage, and reduce the thermal environmental impact caused by the construction of photovoltaic power stations in the surrounding areas.

4. CONCLUSION

We used Landsat 8 and Gaofen-1 remote sensing image data to quantitatively study the thermal environment changes of a photovoltaic power station and its surrounding areas in a mountainous area of Hebei Province. The results show that there is a significant positive correlation between the proportion of photovoltaic power stations and the average land surface temperature under specific geographical and temporal conditions. Photovoltaic power stations are identified as one of the main factors contributing to temperature rise in mountainous areas and exhibit characteristics of traditional heat island effects. In addition, this study provides a brief analysis of the reasons

for temperature rise caused by photovoltaic power stations and proposes effective measures to improve the thermal environment of photovoltaic power stations and their surrounding areas, providing valuable references for addressing the thermal environmental issues of photovoltaic power stations. It should be noted that there are two main sources of error in this study: the low spatial resolution of the Landsat 8 satellite may lead to certain errors in land cover classification results, which may affect the accuracy of subsequent analysis results. In the process of temperature inversion in the study area, the selected thermal infrared image has a relatively low spatial resolution, and the scope of the study area and the research object is small. This may result in a certain deviation between the inverted land surface temperature and the actual land surface temperature, which may affect the accuracy of subsequent analysis.

ACKNOWLEDGEMENTS

This research was funded by the National Natural Science Foundation of China (Grant Numbers 42201483) and the China Postdoctoral Science Foundation (Grant Numbers 2022M710332).

REFERENCES

Broadbent, A.M., Krayenhoff, E.S., Georgescu M., et al.,2019：The observed effects of utility-scale photovoltaics on near-surface air temperature and energy balance. *Journal of Applied Meteorology and Climatology*, 58(5), 989-1006.

Feng Y.J.,2018. The largest mountainous photovoltaic project activates the "photovoltaic+" effect. *Agricultural Engineering Technology*,07(18),36-38.

Genchi Y., Ishisaki M., Ohashi Y., et al.,2003. Impacts of large-scale photovoltaic panel installation on the heat island effect in Tokyo. Fifth Conference on the Urban Climate, Tokyo, Japan.

Janssen, L.L.F., Wel., F, J.M., 1994：Accuracy assessment of satellite derived land-cover data: a review. *Photogram metric Engineering and Remote Sensing*,60(4),419-426.

Lin, T.Y., Dollar P., Girshick R., et al., 2017. Feature Pyramid Networks for Object Detection.The IEEE Conference on Computer Vision and Pattern Recognition (CVPR), pp:2117-2125.

Nemet, G.F.,2009：Net radiative forcing from widespread deployment of photovoltaics. *Environmental Science & Technology*, 43(6),2173-2178.

National Bureau of Statistics of China,2021: 2020 China Statistical Yearbook. Statistical Theory and Practice, Zhengzhou.
Yang, L.W.,2015. Study on Local Microclimate Effects of Large-scale Photovoltaic Power Plants in Golmud Desert Region. University of Chinese Academy of Science, Beijing, China.

Yin, D.Y., Ma L., Qu, J.J., et al. 2017：Impact of Large-scale Photovoltaic Power Plants on Microclimate in the Gonghe Basin Desert Region. *Bulletin of Soil and Water Conservation*,37(3),15-21.

Zhai, H., Larsen, H., Millstein, D., et al., 2012：The potential for avoided emissions from photovoltaic electricity in the United States. *Energy*, 47(1),443-450.

Zhang, Q., Xin, X.Z., et al.2018：Suitability analysis of photovoltaic power station construction in China based on remote sensing data and multi-factor evaluation. *Journal of Geo-information Science*,20(1),119-127.